Int J Adv Manuf Technol (2013) 69:1389–1401
DOI 10.1007/s00170-013-5098-3

ORIGINAL ARTICLE

The influence of organobentonite clay on CO_2 laser grooving of nylon 6 composites

Arkadiusz J. Antończak · Maciej Nowak · Konrad Szustakiewicz · Jacek Pigłowski · Krzysztof M. Abramski

Received: 27 January 2013 / Accepted: 27 May 2013 / Published online: 19 June 2013

Abstract The popular polycaprolactam (polyamide PA6), commonly referred to as nylon 6, widely used as a construction plastic, is not a typical material for micromachining by CO_2 laser vaporization. In this paper, we describe investigations of the pulsed CO_2 laser grooving of both the chemically pure and the organobentonite clay modified nylon 6. Our results indicate that doping of nylon 6 with nanoparticles of organophilized bentonite significantly improves the grooving ability, predictability of the process, and its quality. In order to determine the nature of the changes in the depth and width of the grooves as a function of the laser process parameters, theoretical modeling of the laser grooving of nylon was carried out. The basic parameters of the laser grooving process versus laser beam intensity, pulse repetition rate, scanning speed of the material and various compositions of the organophilized bentonite dopant are presented. Additionally, an example of a three-dimensional engraving/milling of tested materials as well as the impact of doping on the channel profile are examined. The modification of nylon 6 by appropriate doping with bentonite clay radically improves the quality of micromachining with a CO_2 laser.

Keywords Polycaprolactam · Polyamide PA6 · Nylon 6 · Tarnamid · Laser grooving · Laser vaporization · CO_2 laser · Bentonite · Organobentonite

A. J. Antończak (✉) · M. Nowak · K. M. Abramski
Laser and Fiber Electronics Group, Faculty of Electrical Engineering, Wroclaw University of Technology, Wyb. Wyspianskiego 27, 50-370, Wroclaw, Poland
e-mail: arkadiusz.antonczak@pwr.wroc.pl

K. Szustakiewicz · J. Pigłowski
Polymer Engineering and Technology Division, Faculty of Chemistry, Wroclaw University of Technology, Wyb. Wyspianskiego 27, 50-370, Wroclaw, Poland

1 Introduction

The nature of the processes induced by laser irradiation in a target material is determined by the combination of the optical, mechanical, and thermodynamic properties of the material as well as the laser parameters such as wavelength, pulse duration, and fluence. The effects of laser irradiation of organic solids can be divided into two main categories: vibrational excitation and photochemically induced fragmentation. Vibrational excitation can occur both with infrared IR as well as with ultraviolet UV irradiation. In addition, the ultraviolet can also photo-fragment the molecule when the laser energy is expended in breaking the chemical bonds [1]. In both cases, the ablation starts when the density of broken bonds at the surface reaches a certain critical value.

Typically, laser processing of polymers is performed using excimer lasers: 157–355 nm [2], 248 nm [3], 308 nm [4]; solid-state lasers with fundamental or harmonics generation: 395/790 nm [5], 532/1,064 nm [6], 1,064 nm [6, 7]; and CO_2 lasers 10.6 μm [4, 8–12]. In terms of the laser pulse duration, both ultra-short (femtosecond [13], and picosecond [14]), as well as long (microsecond) or continuous operation lasers [8–12] can be utilized. The main motivation for the use of ultra-short pulses is the reduction of the heat-affected zone HAZ due to the shorter duration of the heat source, or the improvement of light absorption resulting from nonlinear effects such as multiphoton absorption [15]. Unfortunately, the cost of investment for this type of lasers is still quite high, which severely limits the use of this technology in industrial processing of such materials. Otherwise, for pulsed CO_2 laser radiation, the interaction with a polymer has a thermal character. The mechanism of material removal in CO_2 laser machining of polymers is mainly a combination of melt shearing and vaporization, of which one may dominate in any particular material. In most of the thermoplastic polymers (such as polyethylene, polypropylene, polystyrene, nylon, etc.), melt shearing prevails and the material is

removed by blowing the molten material from the cutting kerf [8, 16]. Cutting or grooving through vaporization requires, relatively, twice more energy as compared to fusion cutting. One of the most commonly used polymers which is generally cut by laser through vaporization is the poly(methyl methacrylate) PMMA.

There are many scientific articles presenting laser processing of various neat polymers (without fillers): for example polytetrafluoroethylene [8, 14], polyethylene [5, 9, 10], polycarbonate [3, 9–11], PMMA [3, 7, 10, 11], polyetheretherketone [3, 14], as well as fiber-reinforced polymers [12, 17], but there is still a lack of information on nylon grooving properties through vaporization by infrared lasers.

Laser grooving of polymers is used in various manufacturing applications, such as the creation of microchannels for microfluidic systems and biomedical applications, slots for assembly, while in the form of laser scribing is used for part identification marking. The mechanism of laser grooving also takes place in the 3D laser machining (turning, milling) [18–20].

The main problem with laser processing of nylon by evaporation in the IR range (with a CO_2 laser) results both from the high decomposition temperature of the polymer (~327 °C) and from the high mass flow rate (low viscosity) of the molten material. The melt mass flow rate (MFR) for unfilled (pure) nylon 6 (35.5 g/10 min [230 °C/5 kg]) is normatively about ten times higher than that for the PMMA (commonly grooved by laser through vaporization). When the material being processed reaches the evaporation temperature in the zone of influence of laser radiation, strong flow and deformation of the molten material occur in the heat-affected zone. We established that the mass flow rate for the organobentonite-filled nylon is significantly lower, while the modification has also a positive effect on other physical characteristics of the material. Several descriptions of the influence of organobentonite clay on the mechanical properties of nylon 6 can be found in the literature [21, 22], or other nano-fillers (nano-$CaCO_3$) on the milling properties of polyamide [23], but there is no information on how it affects the laser machining of these composites.

This inspired us to carry out research on the influence of organobentonite clay on the laser grooving properties of a nylon-based composite. Our goal was to develop the technology of grooving and cutting of polyamides or its composites with cheap and commonly used CO_2 lasers. For the purpose of our research, we decided to use a commercial, direct writing plotter system with a CO_2 laser, available at moderate prices and therefore widespread in industrial applications.

The selection of nylon 6 as a testing material was also motivated by its practical values. Polyamides are widely used as construction materials. Their key characteristics include: high mechanical strength (rigidity and hardness), high impact strength, high vibration damping capacity, good fatigue strength, very good sliding properties, abrasion resistance, low friction coefficient, high thermal resistance, high chemical resistance (especially to organic solvents, oils, lubricants, and fuels), self-extinguishing properties (fire retardant properties), good electro-insulating and optical properties.

2 Preparation of PA6-clay composites

The base testing material used in our research was nylon 6 (PA6) with a melt volume rate of 120 g (270 °C/5 kg, cm^3/10 min) and a density d=1.14 g/cm^3, supplied under the trade name of Tarnamid (T-27) by Zaklady Azotowe Tarnow (Poland). Organically modified bentonites under the trade name of NanoBent ZW1 (CEC 85 meq/100 g, d_{001}=1.8 nm), supplied by ZMG Zebiec (Poland) were used as a filler.

Composites of PA6 and organically modified clay (PA6 with a clay content of 2.5, 5.0, 7.5, and 10 wt%) were obtained in the extrusion process. Before extrusion, PA6 was dried for 48 h at 80 °C under vacuum. The organobentonite (ZW1) was also dried before compounding, for 4 h and at 60 °C. The nanocomposites were obtained in air atmosphere using a co-rotating twin-screw Brabender DSE 20/40 extruder (D=20 mm, L/D=40). Rotational speed of the screws was set at 250 min^{-1} and the temperature range was 220–240 °C. After extrusion, the extrudates were cooled down in water to 80±5 °C and then pelletized. The neat PA6 was also extruded to ensure the same thermomechanical history of all the investigated samples. Samples for laser micromachining (bars of 98×15×1.1±0.15 mm) were prepared with an Arburg 221M injection molding machine with a barrel temperature ranging from 230 °C (feed) to 260 °C (die) and the injection pressure of 1,500 bar.

3 Physical properties of tested materials

Before starting the laser grooving tests, the impact of doping on the properties of the material was examined. The mechanical properties of all the composites were determined according to the PN-EN ISO 527–1 standard. The tests, including the tensile modulus and the tensile strength, were carried out using the Tira Test 2705 universal strength machine. All the mechanical properties were averaged from at least 20 specimens. Samples for mechanical tests were prepared by an injection molding process. Differential scanning calorimetry (DSC) measurements were carried out on a Mettler Toledo DSC 821 apparatus. All PA6 samples were heated to the melt point to ensure uniform conditions at the

beginning (25–260 °C, heating rate 10 °C/min) to destroy all crystallites, then cooled down to 25 °C with a cooling rate of 10 °C/min. The temperature program was repeated, and the second scan was recorded. The DSC method was used to determine the influence of all the fillers on the melting temperature (T_m) and fusion heat to calculate the degree of crystallinity (X_c). The percent of crystallinity was calculated based on the perfect crystal fusion heat of 190 J/g [24]. MFR measurements were conducted at 230 °C /5 kg using a Zwick plastometer. The mechanical properties of composites are given in Table 1.

Our data analysis leads to the conclusion that the addition of the ZW1 clay leads to an increase of the tensile modulus. This increase is proportional to the filler content and rises up to 52 % as compared to the unfilled PA6. A general conclusion is that all the nanocomposites exhibit much better mechanical properties than the neat PA6. The tensile strength of all the composites is also higher than that of the neat PA6. The highest value of tensile strength, ~13 % higher than for the neat PA6, was obtained for PA6+5 % ZW1. A higher filling level in the composites leads to a decrease of the tensile strength; however, even at a 10 % ZW1 content, the value is still higher than for the PA6. The MFR value decreases with an increasing filling level. This indicates that all the composites have a higher viscosity than the PA6. The MFR value is inversely proportional to the filler content of nanocomposites. Melting temperature (T_m) and the degree of crystallinity are comparable for all the systems.

4 Theoretical model of grooving

Theoretical modeling of laser grooving of nylon was conducted only to determine the nature of the changes, both in the grooves depth and width, as a function of the laser process parameters. For this purpose, the model based on energy conservation proposed by Yuan and Das was adapted [25]. The model used to predict the geometry of a laser grooving or cutting by evaporation of the material is based on the energy balance and assumes that all of the absorbed laser energy (taking into account absorptivity) is converted to heat instantly. When the material reaches the evaporation temperature T_v, or more precisely, the decomposition temperature T_d, it consumes some latent heat L_d. Exceeding the decomposition temperature in the molten phase of thermoplastics, the macromolecules start to decompose due to intensive thermal oscillations. In order to simplify the analysis, the following assumptions were made, which will not substantially affect its accuracy [25, 26]:

(a) The laser beam has a Gaussian intensity distribution,
(b) The laser beam diameter is constant and equal to the beam waist – $2\omega_0$,
(c) The scanning speed of the material is constant,
(d) The material is isotropic with constant thermal and optical properties,
(e) Evaporated material is transparent and does not interfere with incident laser beam,
(f) The effects of polarization are not considered,
(g) Heat losses by convection and radiation from the surface are negligible.

Figure 1 shows the laser grooving process according to which the calculations were made.

Shown in Fig. 1, the complex groove surface, can be separated into a finite surface elements dS described by:

$$dS = \sqrt{1 + tg^2\theta + tg^2\phi}\,dxdy, \tag{1}$$

where θ and ϕ are the inclination angles of the elementary surface, respectively in the x- and y-axis direction (plane of the material). For each element, taking into account the assumptions (g), the energy balance can be defined as follows: the absorbed laser input energy is equal to the sum of the energy that conducts into the finite surface element and energy necessary for the decomposition of the material:

$$E_L dxdy = E_C dS + E_D dxdy, \tag{2}$$

where E_L is the incident laser energy density, E_C is the conductions into the surface element and E_D is the energy density utilized to decompose the polymer. For the Gaussian energy distribution, the laser intensity (two times higher than is often assumed) is given by:

$$I(x,y) = \frac{P}{\pi\omega_0^2/2}\exp\left[-\frac{2}{\omega_0^2}\left(x^2+y^2\right)\right], \tag{3}$$

where P is the average laser power, ω_0 is the beam radius (it

Table 1 Selected properties of PA6 T-27 and PA6+ZW1 nanocomposites

Sample	Young's modulus [MPa]	Tensile strength [MPa]	MFR [230 °C/5 kg] [g/10 min]	T_m [°C]	X_c [%]
PA6 T-27 CF40	$2{,}624_{\pm 48}$	$83.1_{\pm 1}$	35.5	221	31.0
PA6+2.5 % ZW1	$2{,}890_{\pm 47}$	$84.2_{\pm 1}$	25.6	219	31.0
PA6+5.0 % ZW1	$3{,}327_{\pm 38}$	$94.3_{\pm 2}$	14.3	214	28.5
PA6+7.5 % ZW1	$3{,}714_{\pm 46}$	$92.2_{\pm 2}$	6.9	215	29.0
PA6+10.0 % ZW1	$3{,}985_{\pm 58}$	$86.7_{\pm 2}$	6.7	217	29.0

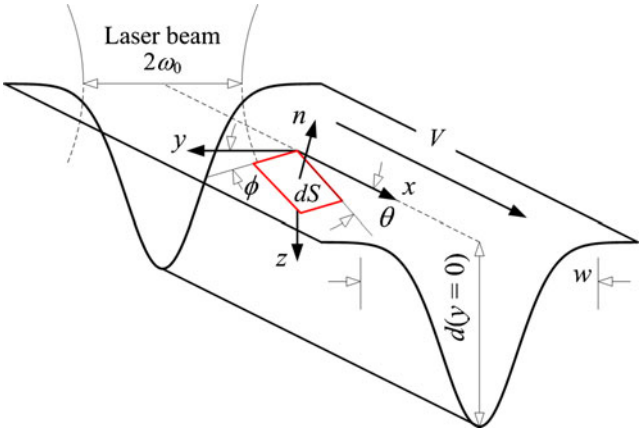

Fig. 1 Schematic of the laser grooving process and definition of the finite surface element

was assumed that $\omega(z)$=const=ω_0). Taking into account the absorptivity a of the material (defined as the fraction of incident radiation absorbed by the material: $a=1-R$, where R is the reflectivity), the laser input energy density can be calculated as:

$$E_L = \int_{-\infty}^{\infty} \frac{2aP}{\pi\omega_0^2} \exp\left[-\frac{2}{\omega_0^2}\left(x^2+y^2\right)\right]\frac{dx}{V} = \sqrt{\frac{2}{\pi}}\frac{aP}{\omega_0 V}\exp\left[-\frac{2y^2}{\omega_0^2}\right], \tag{4}$$

where V is the scanning speed of the material. In turn, the energy conducted into the finite surface dS can be described as the product of the heat flux Φ_q and the time dx/V as follows:

$$E_C dS = \left(\int_{-\infty}^{\infty} -k\left(\frac{\partial T}{\partial n}\right)\Big|_{n=0}\frac{dx}{V}\right)dS, \tag{5}$$

where $k=\alpha\rho c$ is the thermal conductivity, α is the thermal diffusivity, ρ is the density of the material and c is the specific heat of the material. For a heat source moving with velocity V in the x direction, the heat transfer equation can be written as [15, 26]:

$$\nabla^2 T = \frac{\partial^2 T}{\partial n^2} = \frac{V}{\alpha}\frac{\partial T}{\partial x}. \tag{6}$$

Substituting equations resulting from the geometry shown in Fig. 1 yields:

$$\frac{\partial T}{\partial x} = \frac{\partial T}{\partial z}\tan\theta\ , \quad \frac{\partial T}{\partial y} = \frac{\partial T}{\partial z}\tan\phi, \quad \frac{\partial T}{\partial n} = \sqrt{\left(\frac{\partial T}{\partial x}\right)^2+\left(\frac{\partial T}{\partial y}\right)^2+\left(\frac{\partial T}{\partial z}\right)^2}, \tag{7}$$

the heat transfer Eq. (6) can be written as:

$$\frac{\partial^2 T}{\partial n^2} = \frac{V\tan\theta}{\alpha\sqrt{1+\tan^2\theta+\tan^2\phi}}\frac{\partial T}{\partial n}. \tag{8}$$

Taking into account the boundary conditions: $T=T_d$ at $n=0$ and $T=T_e$ at $n=\infty$ (semi-infinite model), where T_e is the ambient temperature and T_d is the decomposition temperature, the temperature gradient at the surface dS is given by:

$$\frac{\partial T}{\partial n}\Big|_{n=0} = -\frac{V\tan\theta(T_d-T_e)}{\alpha\sqrt{1+\tan^2\theta+\tan^2\phi}}. \tag{9}$$

Substituting Eq. (9) into Eq. (5), the conduction energy becomes:

$$E_C dS = \rho c(T_d-T_e)d(y)dxdy. \tag{10}$$

The last component of the energy balance equation, the decomposition energy, can be written as:

$$E_D dxdy = \rho L d(y)dxdy, \tag{11}$$

where L_d is the latent heat of decomposition and $d(y)$ is the depth of the groove at y position. The above considerations neglect the latent heat of fusion, because it is an order of magnitude smaller than the heat of decomposition. Substituting Eqs. (4), (10), and (11) into Eq. (2), the depth of the groove can be calculated as:

$$d(y) = \sqrt{\frac{2}{\pi}}\frac{aP}{\omega_0 Q\rho V}\exp\left[-\frac{2y^2}{\omega_0^2}\right], \tag{12}$$

where $Q=c(T_d-T_e)+L_d$ is the specific energy. The maximum depth of the grove is obtained at the laser beam centerline by putting in Eq. (12) $y=0$. The above Eq. (12) is true both for continuous wave (CW) laser operation [25], as well as for long pulse quasi-CW operation [7]. In the case of CW laser operation, the depth of the groove is represented as a function of the laser power and scanning speed of the material, while in the Q-CW pulse operation one can use overlap between successive laser pulses O_v as a alternative variable for scanning speed V [for a particular pulse repetition rate (PRR)]. Taking into account the relationship between the scanning speed of the material V, the pulse repetition rate PRR of the laser and the degree of overlap between successive laser pulses O_v defined as:

$$O_V = 1-V\Big/(2\omega_0 PRR). \tag{13}$$

Taking into account Eq. (13) the depth $d(y)$ of the groove can be expressed as:

$$d(y) = \frac{aP}{\sqrt{2\pi}\omega_0^2 Q\rho\cdot PRR\cdot(1-O_V)}\exp\left[-\frac{2y^2}{\omega_0^2}\right]. \tag{14}$$

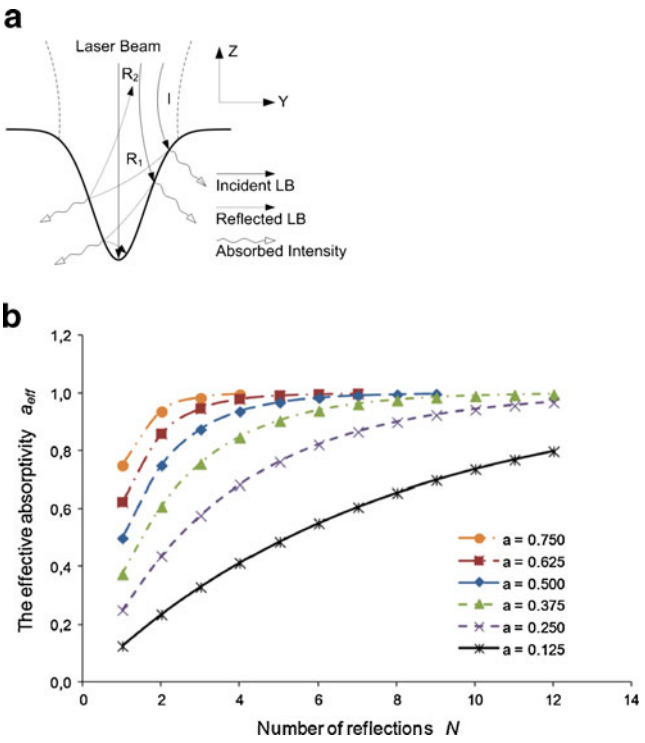

Fig. 2 The multiple reflection phenomena: **a** a symbolic diagram, **b** the effective absorptivity as a function of multiple reflections, for several values of the initial absorptivity

The width of the groove can be calculated based on the material ablation threshold [26]. Using Eq. (3) it is possible to determine the threshold value of the intensity of the laser beam I_{th}, which causes a visible change in the material in an area with a radius of y_{th} (for x=0):

$$I_{\text{th}} = \frac{P}{\pi\omega_0^2/2}\exp\left[-\frac{2y^2}{\omega_0^2}\right]. \tag{15}$$

On the other hand, the threshold value of the beam intensity I_{th} can be defined as the ratio of the ablation threshold F_{th} of the material to the time of irradiation t_{ir}:

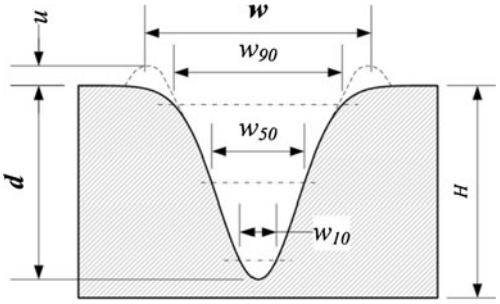

Fig. 3 A typical cross-section of laser grooving with emphasized characteristic parameters: H is the thickness of material, d is the depth of grooving, w is the inlet width of the groove (on the surface of the material), w_{10} , w_{50}, and w_{90} are the widths at: 10, 50, and 90 % of the total depth, respectively, u is the uplift of the ejected material

$$I_{\text{th}} = \frac{F_{\text{th}}}{t_{ir}} = \frac{F_{\text{th}}V}{2\omega_0}. \tag{16}$$

Comparing Eqs. (15) and (16) the width of the groove can be defined as:

$$w = 2y = \sqrt{2}\cdot\omega_0\sqrt{\ln\frac{4P}{\pi\omega_0 F_{\text{th}}V}} = \omega_0\sqrt{2\cdot\ln\frac{F}{F_{\text{th}}}}, \tag{17}$$

where F=$4P/\pi\omega_0 V$ is the laser fluence.

The depth of the groove estimated from the formula (12) was slightly different from that from the experimental data. A similar difference was also noted by a few authors [27, 28]. This results from many factors. One of the most important reasons for this discrepancy is the variability of the effective absorptivity of the material as a function of the temperature of the material [15], the depth of the grooves [29], the duration of the process [30] and the geometry of the laser beam (focusing optics) [16]. Once the material melts, the absorptivity increases dramatically and essentially becomes independent of the wavelength [15]. A part of the laser radiation not absorbed in the formed groove can be re-absorbed due to multiple reflections from the side surfaces of the channel [30]. The degree of enhancement of the absorptivity due to multiple reflections depends on the

Table 2 Material properties of the PA6 used for calculations

Parameter	Symbol / unit	Value	References
Beam waist	ω_0 [μm]	62.5	Measured
Density	ρ [kg/m^3]	1,140	Measured
Specific heat	c [J/K·kg]	1,550	[33, p.75]
Ambient temperature	T_e [°C]	25	Measured
Decomposition temperature	T_d [°C]	327	[34]
Latent heat of decomposition	L_d [kJ/kg]	1,500	[33, p.73]
Normalized absorptance	a [−]	~0.12[a]	[31, p.398]
Ablation threshold	F_{th} [kJ/m^3]	450	[4]

[a] Value obtained from the graph

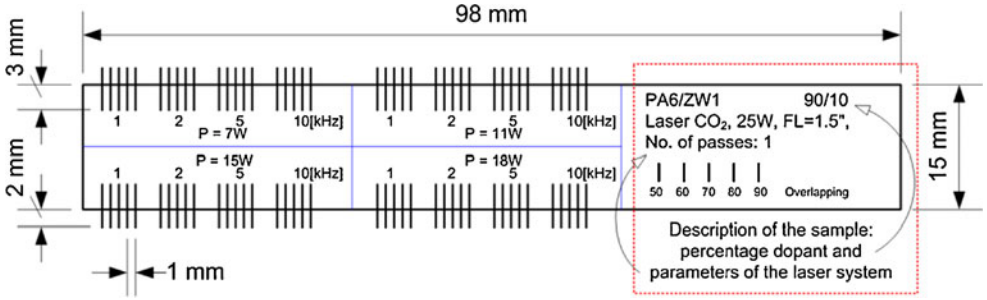

Fig. 4 Test layout for the sets of lines with different process parameters

particular geometry and dimensions of the groove. Symbolically, this situation is shown in Fig. 2a.

Under a simplifying assumption that the absorptivity does not depend on the angle of incidence of the radiation, the effective absorptivity a_{eff} (shown in Fig. 2b) due to multiple reflections N can be simply written as [30]:

$$a_{eff} = \sum_{1}^{N} a(1-a)^{n-1}. \tag{18}$$

Therefore, regardless of whether it is taken as the value of the material absorptivity, the absorptivity measured spectrometrically for cold material (Nylon 6, $a \approx 0.12$ [31]), or the absorptivity measured calorimetrically [15] at specific, fixed values of laser process parameters (e.g. Nylon 6, $a=0.9203$ [27]), each time an adjustment of the theoretical model will be necessary due to the factors described above. In order to make a correct predication of the depth of the groove, Eq. (12) was modified by introducing two analytical constants γ and β as follows [27, 28]:

$$d(y) = \gamma\sqrt{\frac{2}{\pi}\frac{a}{\omega_0 Q\rho}}\left(\frac{P}{V}\right)^{\beta}\exp\left[-\frac{2y^2}{\omega_0^2}\right], \tag{19}$$

or for $y=0$ (the maximum depth of the grove):

$$d_{\max} = \gamma\sqrt{\frac{2}{\pi}\frac{a}{\omega_0 Q\rho}}\left(\frac{P}{V}\right)^{\beta}, \tag{20}$$

where γ and β are constants related to material properties and laser focusing optics configuration. The values of both parameters were determined experimentally based on the approximation of the measurement results for the undoped nylon using nonlinear Eq. (20) as: $\gamma=1.48$ and $\beta=1.04$. These parameters directly show the differences between the experimental data and the theoretical model. The ideal case: $\gamma=1$, $\beta=1$ – would mean that there are no differences.

The analytical calculations were carried out according to the model. Because of the slight differences in the width and depth of the grooves for all tested materials ~5 % (neglecting the geometry distortions arising from the flow of undoped nylon) and due to the difficulty in determining all the physical parameters of the composites (necessary for this analysis), the calculation was performed only for the unfilled (neat) nylon. The physical parameters of the PA6 used for calculation are listed in Table 2.

5 Experimental details

The geometry of laser grooving (a typical profile is shown in Fig. 3) can be characterized mainly by four parameters: d

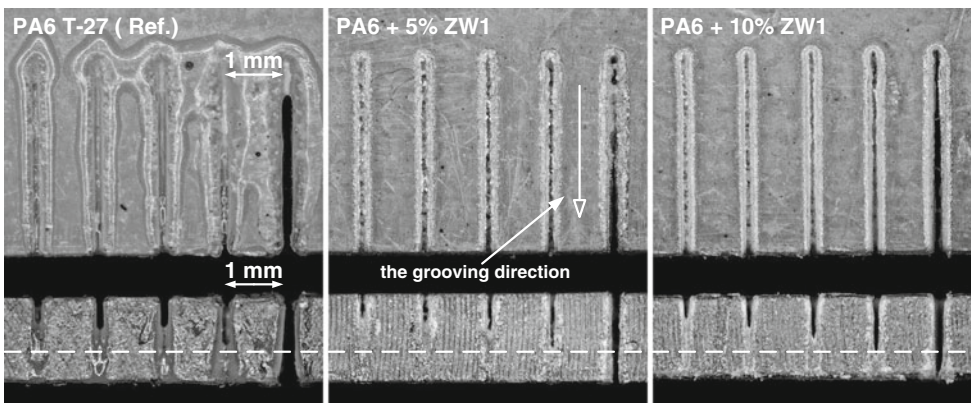

Fig. 5 Microscope profile and cross-section of grooving line in the PA6 and the PA6 nanocomposites, from *left* to *right*: **a** for the neat (unfiled) PA6 (T-27), **b** for the 5 % ZW1 organobentonite-doped PA6, **c** for the 10 % ZW1 organobentonite-doped PA6. Parameters of the laser beam: average output power $P=18$ W, pulse repetition rate PRR = 1 kHz, and five levels of overlap of the laser pulse (from *left* to *right*, 50, 60, 70, 80, and 90 %, respectively), one pass process

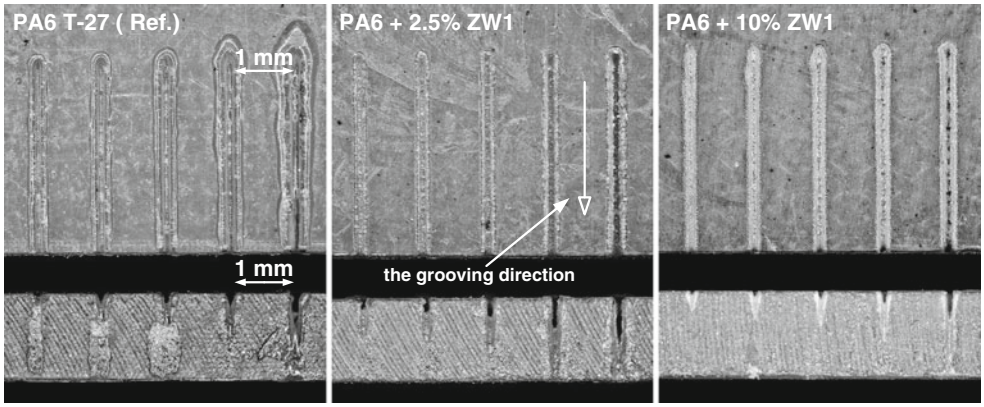

Fig. 6 Microscope profile and cross-section of grooving line in the PA6 and the PA6 nanocomposites, from *left* to *right*: **a** for the neat (unfiled) PA6 (T-27), **b** for the 2.5 % ZW1 organobentonite-doped PA6, **c** for the 10 % ZW1 organobentonite-doped PA6. Parameters of the laser beam: average output power $P=18$ W, pulse repetition rate PRR=5 kHz, and five levels of overlap of the laser pulse (from *left* to *right*, 50, 60, 70, 80, and 90 %, respectively), one pass process

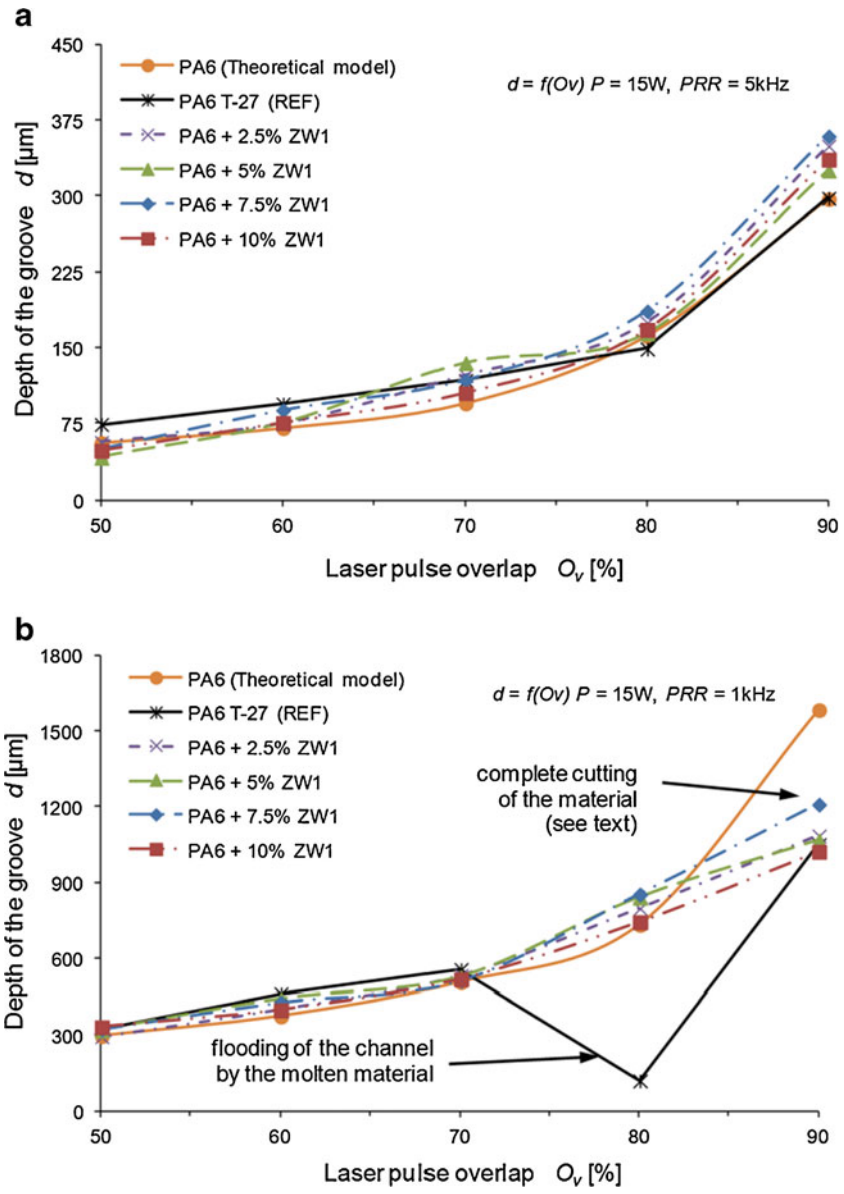

Fig. 7 Depth of groove as a function of overlap between successive pulses: **a** for the average laser output power $P=9$ W and the pulse repetition rate PRR=5 kHz, **b** for $P=15$ W and PRR=1 kHz

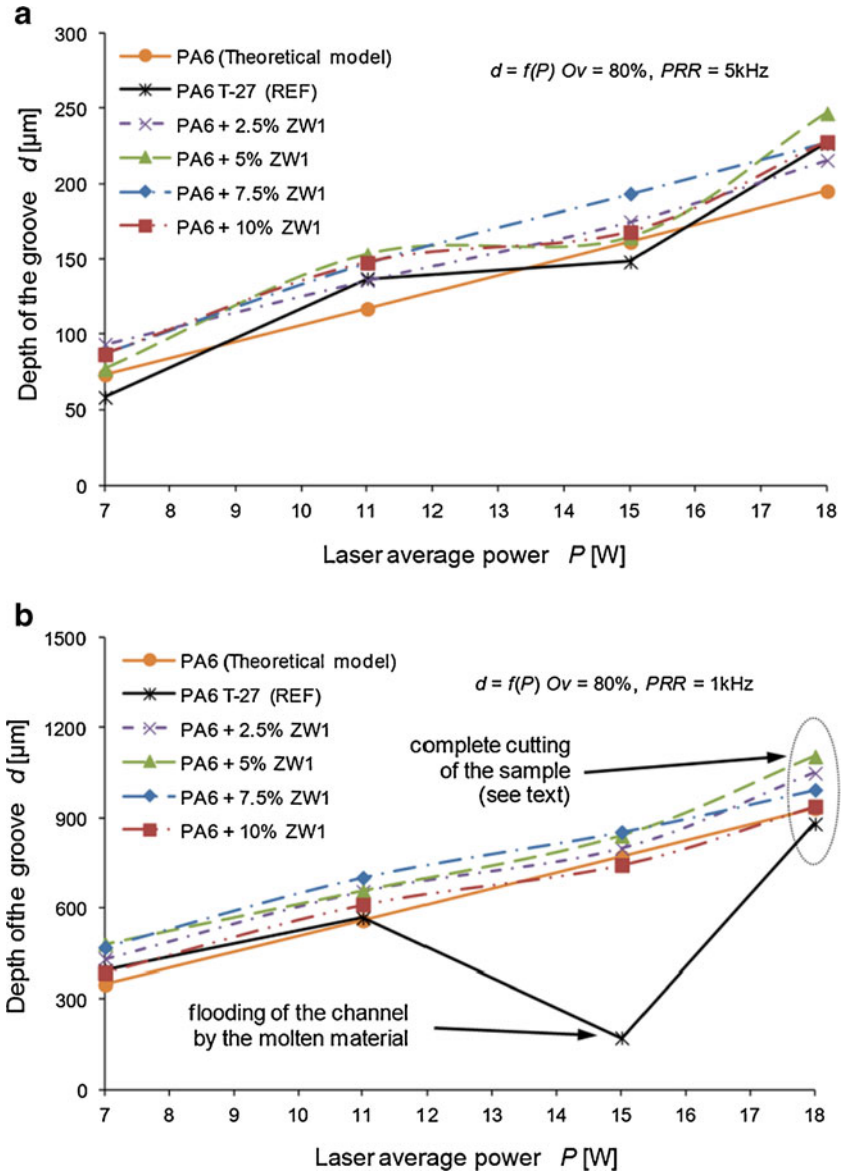

Fig. 8 Depth of groove as a function of the laser average output power P: **a** for the overlap of the laser pulse O_V=80 % and the pulse repetition rate PRR=5 kHz, **b** for O_V=80 % and PRR=1 kHz

depth, w width, u uplift (caused by material ejected from the groove) and the taper – t_p. Taper is a measure of the slope of the walls against the main plane of the grooving object and is defined as follows:

$$t_p = \arctan\left(\frac{w_{90}-w_{10}}{2d}\right), \tag{21}$$

where d is the depth of grooving and w_{10}, w_{90} are the widths at 10 and 90 % of the total depth, respectively.

Taper can be either positive ($w_{90}>w_{10}$) or negative ($w_{90}<w_{10}$). The ideal (often very important) case requires the situation where $w_{90}\sim w_{10}$. In fact, for most cases and materials the taper is positive. Nevertheless, negative taper can also occur, namely when the interaction between the laser beam and the material is too strong, causing a broadening (due to reabsorption) at the bottom of a grooving space.

In order to perform the experiments, a special test layout pattern was prepared. The test contains all the essential parameters of laser processing (average power, overlap of the laser pulse, and pulse repetition rate). An example of a test layout is given in Fig. 4 which shows a set of straight lines perpendicular to the edge and characterized by different parameters. In order to have a fully clear picture of grooving, the process always started from the layout inside towards its edge. In this way, we had an opportunity to observe the edge and the quality of grooving by microscope. The measurements of the grooving profiles geometry were performed with a digital microscope, the Keyence VHX-1000E.

For the purpose of the experiment, as a laser micromachining system, a commercial plotter system based on a RF excited CO_2 laser (Synrad, series 48-2) [32] with a maximum average output power of 25 W was used. The output power was controlled by

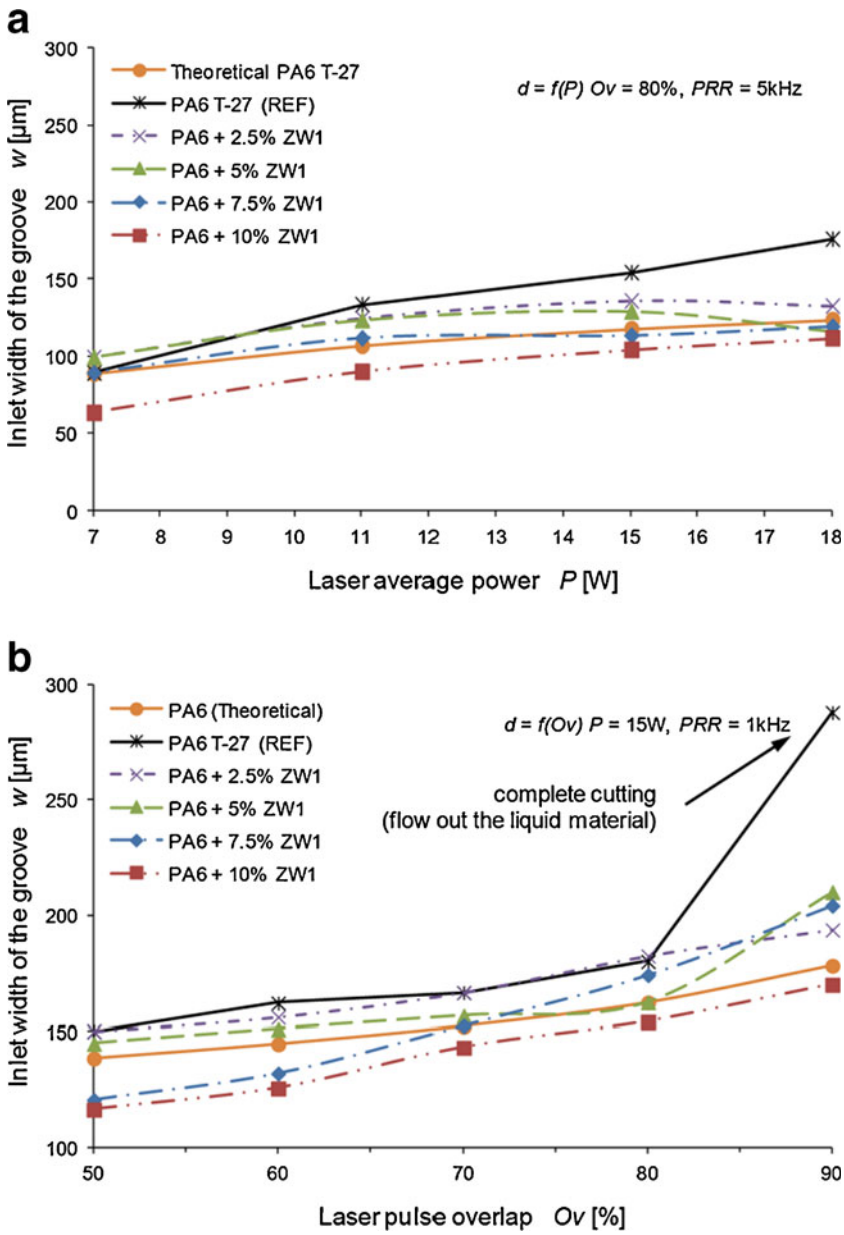

Fig. 9 Inlet width of groove as a function of: **a** the average laser output power P (at O_V=80 %, PRR=5 kHz), **b** the overlap of the laser pulse O_v (at P=15 W, PRR=1 kHz)

changing the duty cycle DC of pulses that modulate the RF power delivered to the laser head. Since the laser was not wavelength-stabilized, it could operate at one of the four spectral lines P18, P20, P22, or P24 (10.57–10.63 μm) with mostly dominating P20 line. The minimum spot size of the laser beam was estimated at about 125 μm for the 1.5″ focusing lens of the system. The quality factor of the laser beam was M^2<1.2.

6 Tests and results

For laser grooving tests, we used a combination of four values of the average laser power P (7–18 W), five values of the overlap of the laser pulse O_v (50–90 %), and four values of the pulse repetition rate PRR (1, 2, 5, and 10 kHz). Some representative results of grooving are shown in Figs. 5 and 6.

The initial (visual) analysis shows that for the organobentonite clay (ZW1) doped nylon (PA6) with a 5 or 10 % level of ZW1 doping, the properties of the laser grooving improve significantly. Furthermore, as indicated in Fig. 5 (white dashed line) the depths of the grooves for the same parameters are quite comparable. It is clearly seen that for pure nylon the quality of grooving is very poor—lines are deformed (e.g. Figs. 5a and 6a) due to melting and flowing of the material in the HAZ; there was a very large HAZ and the taper was unpredictable. All of the above-mentioned phenomena make the CO_2 laser grooving of pure polyamide completely useless. Otherwise, for the composites (doped materials), the HAZ

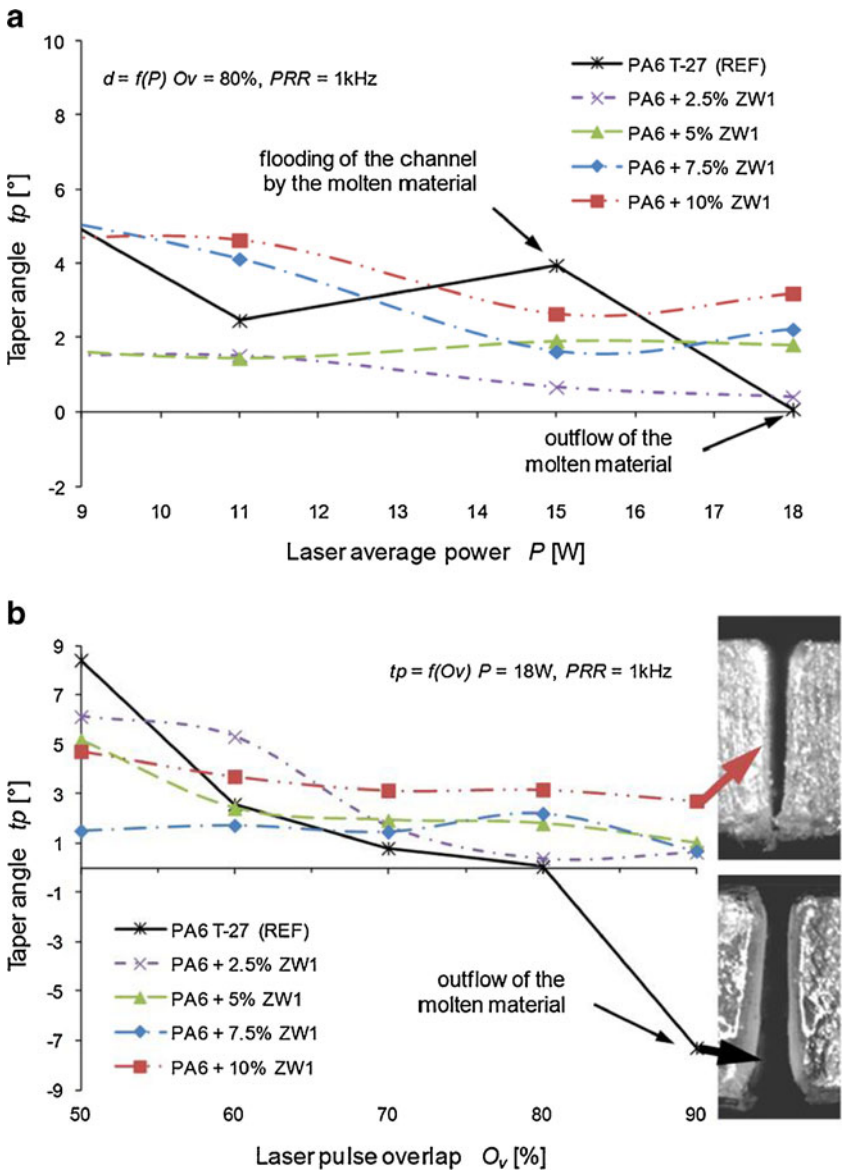

Fig. 10 Taper as a function of: **a** the average laser output power P (at O_V=80 %, PRR=1 kHz), **b** the overlap of the laser pulse O_v (at P=18 W, PRR=1 kHz)

decreases significantly and the grooving process seems to be more predictable. In order to have an objective evaluation of the grooving properties changes due to changes in the laser process parameters, microscopic measurements (Keyence VHX-1000E digital microscope) of depth, width, and taper of the obtained structures were carried out. In none of the analyzed cases, the material uplift appeared, hence this parameter was not measured. The graphs for selected cases are shown in Figs. 7, 8, 9, and 10.

For most of the analyzed cases, the doping of organ-obentonite clay slightly increased the depth of the groove at the same process parameters (Figs. 7 and 8). This results from the differences in the physical properties (mainly the absorptivity) of the composite due to doping. These differences are not as important as the differences in the behavior of the tested materials after exceeding a certain amount of energy. For the pulse repetition rate of 1 kHz, the average power of 15 W or more, and the overlap of the laser pulse of 80 % or more, the undoped material began to flow, causing flooding of the grooved channel (Figs. 7b and 8b). For doped materials this phenomenon does not occur. This is due to the much higher viscosity of these materials. The measured MFR—Table 1—is from 1.4 (for PA6+2.5 % ZW1) to 5.3 (for PA6+10 % ZW1) times smaller than for undoped nylon. Even if the temperature in the HAZ exceeds the melting point, the material retains its form, which has a positive effect on grooving geometry.

For the pulse repetition rate of 1 kHz, the average power of 15 W or more and the overlap of the laser pulse of 80 % or more, a complete intersection of material was observed. Because of the various thicknesses of the test plates (tolerance of±0.15 mm), different values for this case were recorded (Figs. 7b and 8b). These measuring points were placed on the graph only in order to indicate that the material was cut.

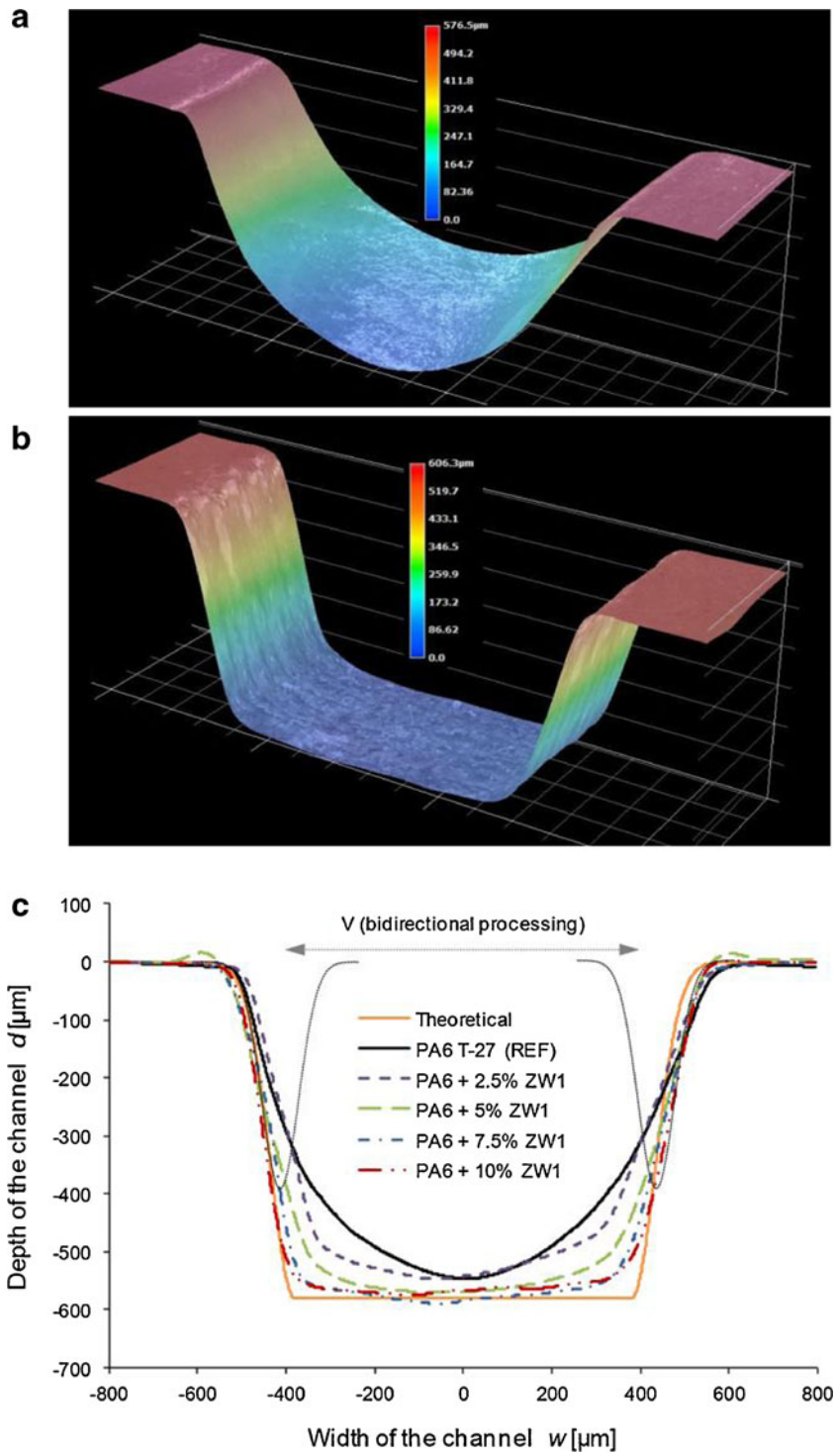

Fig. 11 Channel profiles made in the PA6 and the PA6 nanocomposites depending on the percentage of dopant (organobentonite): **a** the cross-section for pure nylon, **b** the cross-section for 10 % ZW1 doped PA6, **c** the profiles for all tested materials (P=6 W, V=177 mm/s, PRR=3.5 kHz, Keyence VHX-1000E digital microscope)

Similarly, doping was found to have a positive effect on the width of the grooved channel, as can be seen in Fig. 9. Also in this case, the situation is analogous: increased percentage of doping leads to (in most cases) a narrower channel width (see also Fig. 5a, c). Analysis of Eq. (18) shows that this is due to the higher ablation threshold for the dopant materials. For pure nylon, the width of the grooves was greater compared to the theoretical model, and the difference was more significant for higher laser power. This was due to flow of the melt. As before, for pure nylon, the pulse repetition rate of 1 kHz, the average power of 15 W and the overlap of the laser pulse of 90 % (Fig. 9b) due to complete intersection of material a marked increase in the width of the groove was observed. For doped materials this effect does not occur.

The last analyzed parameter was the taper—Fig. 10. For the undoped material (Fig. 10b—solid line), the taper ranges

from a positive value for small overlap of the laser pulse through zero to negative values when the molten material outflows from the cut channel. In the case of composites doped with organobentonite clay, the extent of changes in taper is much smaller (0.5–6°), and its value is always positive. Due to a lower MFR, there is no outflow of molten fraction of the material.

This analysis shows that due to doping, the PA6-based composite becomes appropriate for CO_2 laser grooving with a satisfactory quality. Some inaccuracies in the measurements—the mutual interweaving of plots for different degrees of doping—might be because the prepared test samples were not perfectly homogeneous (because to the way in which they were made). This, however, had no significant effect on the dominant, visible trend.

In addition to the grooves, a three-dimensional engraving / milling test was also performed. In this case, a channel of 0.9 mm in width (nominal value) was made by bidirectional scanning of the material across the length of the channel. Differences in the channel profile for all tested materials, depending on the percentage of doping are shown graphically in Fig. 11 (selected case).

An increase of the degree of doping of nylon-based composites allows to obtain a channel profile closer to the theoretical shape. The maximum difference in channel depth does not exceed 43 μm (<8 % of the total depth). Larger cross-sectional area of the channels in composite materials as compared to the neat PA6 results from the differences in the physical properties (mainly the absorptivity and the ablation threshold) of the material.

7 Conclusions

We showed that the poor quality of grooving through vaporization of neat (unfilled) nylon PA6 T-27 with a CO_2 laser makes it totally unusable, mainly due to the very large HAZ and the unpredictable behavior of the material above a certain value of laser fluence. Our aim was to investigate how the degree of doping improves the quality of the laser grooving properties of nylon with organobentonite clay. As there is no information in the literature about the properties of CO_2 laser grooving of nylon, we assumed that results obtained for the undoped nylon can be treated as a "self-reference" for the other cases (it means nylon with organobentonite). In the case of the composite materials we found out that a 2.5–10 % doping of nylon with organobentonite clay definitely improves the grooving properties, which is due to much lower melt mass flow rate of these materials – up to 5.3 times at 10 % of ZW1 as can be seen in microscopic images. Moreover, all tested composites exhibited much better mechanical properties than neat nylon.

In addition to the grooves, an example of a three-dimensional engraving of tested materials and the impact of doping on the channel profile were examined. We established that increased doping allows to obtain channel profiles closer to the theoretical shape.

As shown, doping allows for a good quality of micromachining of such composites to be achieved with commonly available CO_2 lasers, which might become a fully competitive method as compared to the commonly used methods such as thermoforming and mechanical machining. What is worth noting, neither the modifying materials, nor the CO_2 laser systems are expensive. Doping of high amounts of organobentonite (up to 10 % of ZW1) leads to excellent grooving results and significant elimination of the HAZ effect. Considering the improvement of the material laser processing properties as well as its physical properties (tensile strength), doping at the level of around 5–7.5 % could be considered as optimal.

Acknowledgments This research was supported in part by statutory funds from the Institute of Telecommunications, Teleinformatics and Acoustics, Wroclaw University of Technology, under grant no. S200-10 and also by statutory funds from the Polymer Engineering and Technology Division, Faculty of Chemistry, Wroclaw University of Technology.

References

1. Zhigilei LV, Garrison BJ (2000) Microscopic mechanisms of laser ablation of organic solids in the thermal and stress confinement irradiation regimes. J Appl Phys 88:1281–1298. doi:10.1063/1.373816
2. Bityurin N (2005) Studies on laser ablation of polymers. Annu Rep Prog Chem Sect C Phys Chem 101:216–247. doi:10.1039/B408910N
3. Tokarev VN, Lopez J, Lazare S, Weisbuch F (2003) High-aspect-ratio microdrilling of polymers with UV laser ablation: experiment with analytical model. Appl Phys A 76:385–396. doi:10.1007/s00339-002-1511-8
4. Skordoulis CD, Makropoulou M, Serafetinides AA (1995) Ablation of nylon-6,6 with UV and IR lasers. Appl Surf Sci 86:239–244. doi:10.1016/0169-4332(94)00413-7
5. Okoshi M, Inoue N (2004) Laser ablation of polymers using 395 nm and 790 nm femtosecond lasers. Appl Phys A 79:841–844. doi:10.1007/s00339-004-2815-7
6. Dyer PE, Pervolaraki M, Lippert T (2005) Experimental studies and thermal modelling of 1064- and 532-nm Nd:YVO_4 micro-laser ablation of polyimide. Appl Phys A 80:529–536. doi:10.1007/s00339-004-3085-0
7. Teixidor D, Orozco F, Thepsonthi T, Ciurana J, Rodríguez CA, Özel T (2012) Effect of process parameters in nanosecond pulsed laser micromachining of PMMA-based microchannels at near-infrared and ultraviolet wavelengths. Int J Adv Manuf Technol. doi:10.1007/s00170-012-4598-x

8. Kurt M, Kaynak Y, Bagci E, Demirer H, Kurt M (2009) Dimensional analyses and surface quality of the laser cutting process for engineering plastics. Int J Adv Manuf Technol 41:259–267. doi:10.1007/s00170-008-1468-7
9. Caiazzo F, Curcio F, Daurelio G, Memola Capece Minutolo F (2005) Laser cutting of different polymeric plastics (PE, PP and PC) by a CO_2 laser beam. J Mater Process Technol 159:279–285. doi:10.1016/j.jmatprotec.2004.02.019
10. Davim JP, Barricas N, Conceicao M, Oliveira C (2008) Some experimental studies on CO_2 laser cutting quality of polymeric materials. J Mater Process Technol 198:99–104. doi:10.1016/j.jmatprotec.2007.06.056
11. Choudhury IA, Shirley S (2010) Laser cutting of polymeric materials: an experimental investigation. Opt Laser Technol 42:503–508. doi:10.1016/j.optlastec.2009.09.006
12. Riveiro A, Quintero F, Lusquinos F, del Val J, Comesana R, Boutinguiza M, Pou J (2012) Experimental study on the CO_2 laser cutting of carbon fiber reinforced plastic composite. Compos Part A 43:1400–1409. doi:10.1016/j.compositesa.2012.02.012
13. Womack M, Vendan M, Molian P (2004) Femtosecond pulsed laser ablation and deposition of thin films of polytetrafluoroethylene. Appl Surf Sci 221:99–109. doi:10.1016/S0169-4332(03)00835-3
14. Serafetinides AA, Makropoulou MI, Skordoulis CD, Kar AK (2001) Ultra-short pulsed laser ablation of polymers. Appl Surf Sci 180:42–56. doi:10.1016/S0169-4332(01)00324-5
15. Kannatey-Asibu E Jr (2009) Principles of laser materials processing. Wiley, Hoboken
16. Dahotre NB, Harimkar SP (2008) Laser fabrication and machining of materials. Springer, New York
17. Cenna AA, Mathew P (2002) Analysis and prediction of laser cutting parameters of fibre reinforced plastics (FRP) composite materials. Int J Mach Tool Manu 42:105–113. doi:10.1016/S0890-6955(01)00090-6
18. Li J, Liu C, Ke X, Xu Z, Li M, Duan Y, Fan Y, Wang L (2012) Fabrication of a thermoplastic multilayer microfluidic chip. J Mater Process Technol 212:2315–2320. doi:10.1016/j.jmatprotec.2012.06.022
19. Liu HB, Gong HQ (2009) Templateless prototyping of polydimethylsiloxane microfluidic structures using a pulsed CO_2 laser. J Micromech Microeng 19:037002. doi:10.1088/0960-1317/19/3/037002
20. Stournaras A, Salonitis K, Stavropoulos P, Chryssolouris G (2009) Theoretical and experimental investigation of pulsed laser grooving process. Int J Adv Manuf Technol 44:114–124. doi:10.1007/s00170-008-1818-5
21. Liu X, Wu Q (2002) Polyamide 66/clay nanocomposites via melt intercalation. Macromol Mater Eng 287:180–186. doi:10.1002/1439-2054(20020301)287:3<180::AID-MAME180>3.0.CO;2-T
22. Araujo EM, Melo TJA, Santana LNL, Neves GA, Ferreira HC, Lira HL, Carvalho LH, Avila MM Jr, Pontes MKG, Araujo IS (2004) The influence of organo-bentonite clay on the processing and mechanical properties of nylon 6 and polystyrene composites. Mater Sci Eng B 112:175–178. doi:10.1016/j.mseb.2004.05.027
23. Zinati RF, Razfar MR (2013) An investigation of the machinability of PA 6/nano-$CaCO_3$ composite. Int J Adv Manuf Technol. doi:10.1007/s00170-013-4875-3
24. Xie S, Zhang S, Wang F, Yang M, Seguela R, Lebebvre JM (2007) Preparation, structure and thermomechanical properties of nylon-6 nanocomposites with lamella-type and fiber-type sepiolite. Compos Sci Technol 67:2334–2341. doi:10.1016/j.compscitech.2007.01.012
25. Yuan D, Das S (2007) Experimental and theoretical analysis of direct-write laser micromachining of polymethyl methacrylate by CO_2 laser ablation. J Appl Phys 101:024901
26. Choi WC, Chryssolouris G (1995) Analysis of the laser grooving and cutting processes. J Phys D Appl Phys 28:873–878. doi:10.1088/0022-3727/28/5/007
27. Desai CK, Shaikh A (2012) Prediction of depth of cut for single-pass laser micro-milling process using semi-analytical, ANN and GP approaches. Int J Adv Manuf Technol 60:865–882. doi:10.1007/s00170-011-3677-8
28. Zhou BH, Mahdavian SM (2004) Experimental and theoretical analyses of cutting nonmetallic materials by low power CO_2-laser. J Mater Process Technol 146:188–192. doi:10.1016/j.jmatprotec.2003.10.017
29. Steen WM (1991) Laser material processing. Springer, London
30. Ki H, Mohanty PS, Mazumder J (2002) Multiple reflection and its influence on keyhole evolution. J Laser Appl 14:39–45. doi:10.2351/1.1449885
31. Stuart BH (2007) Analytical techniques in material conservations. Wiley, West Sussex
32. Synrad, Inc. (2011) http://www.synrad.com/48series/48.pdf (datasheets of the 48-series CO_2 laser)
33. Lyon RE, Janssens ML (2005) Polymer flammability. The report of the Federal Aviation Administration William J Hughes Technical Center's. National Technical Information Service (NTIS), Springfield
34. Klein R (2011) Laser welding of plastics—materials, processes and industrial applications. Wiley, Gloucestershire